Digest Journal of Nanomaterials and Biostructures Vol. 8, No. 4, October- December 2013, p. 1461 - 1473

PREFERRED CRYSTAL ORIENTATION IN THIN-FILM NANOCRYSTALLINE SILICON DETERMINED BY RAMAN SPECTROSCOPY

S. N. AGBO[a,b,*], P. SUTTA[a]
[a] *New Technologies Research Centre, University of West Bohemia, 306 14 Plzen, Czech Republic*
[b] *National Centre for Energy Research and Development, University of Nigeria, Nsukka, Nigeria*

In this contribution, we report a unique approach of determining preferred orientation in hydrogenated thin film nanocrystalline silicon (nc-Si:H) using Polarized Raman Spectroscopy (PRS). This method is based on the fact that molecular vibrations in films under polarized light also give rise to polarization-dependent Raman scattered intensity depending on the grain crystal orientation of the irradiated material. First, the dependence of the Raman intensity of the 520 cm^{-1} TO peak on rotation angle is measured on (100), (110), and (111) single-crystalline silicon wafers. We found distinct patterns for these reference wafers and have used these patterns as a fingerprint for a specific crystal orientation in nc-Si:H. Subsequently, we measured the Raman intensity of the TO peak as a function of rotation angle on the deposited nc-Si:H films and compared the obtained patterns with that of the references. We assumed that nc-Si:H is a linear system composed of a mix of crystals of varying orientations and thus we applied the superposition principle. Using the least square fitting routine we obtained the correlation parameters of the different orientations. By comparison of these parameters, the preferred orientations in our samples were inferred and this was further corroborated by x-ray diffraction results.

(Received July 16, 2013; Accepted October 27, 2013)

Keywords: Thin film nanocrystalline silicon, crystal orientation, crystalline mass fraction, Polarized Raman spectroscopy

1. Introduction

Hydrogenated nanocrystalline silicon (nc-Si:H) has been widely applied in tandem solar cells for the efficient utilization of the solar spectrum. It is used as the bottom cell in the so-called micromorph cell where its long wavelength response and stability to light-induced degradation is exploited. This material is mainly composed of crystals, spatially distributed in an amorphous matrix, resulting in a material with a complex structure. The structural and material properties of nc-Si:H largely depend on the crystalline mass fraction and orientation [1]. Insight into film preferred crystal orientation is important as it gives an understanding of the growth process. Furthermore, physical properties such as conductivity are affected by the crystal orientation and the general characteristics of polycrystalline materials are dominated by the properties of the crystals with the dominant or preferred orientation [2].

Various techniques have been used to investigate the structure and composition of nc-Si:H and the preferred orientation of its crystals. X-ray diffraction (XRD) for instance has been widely applied in investigating the crystal structure of nc-Si:H. Transmission electron microscopy (TEM) [3-6] has been applied also to probe the material structure of nc-Si:H. Although well-established, TEM is destructive, time-consuming, and expensive. Similarly XRD is not a fast measurement and the obtained diffraction pattern can easily be affected by impurities [7]. Analysis using computer programs for grain orientation determination from measured traces of crystallographic planes has

* Corresponding author: agbo@ntc.zcu.cz

been used [8]; however this is limited in that it is time-consuming, tedious and often applied only to a specific crystal plane. Raman spectroscopy on the other hand is a fast, non-destructive technique that requires no sample preparation. Raman spectroscopy has a high spectral resolution with added features that allow for surface enhancement, polarization measurement and compatibility with aqueous samples [9]. It has wide application in estimating the degree of stress and disorder in thin-films [6, 10-11] and the crystalline mass fraction, f in nc-Si:H [12]. This quantity gives the fraction of silicon in the material that is in the crystalline phase. The use of Raman for predicting the crystal orientation has been proposed and is based on the intensity dependence of the Raman signal on the directions of the polarization vectors of the incident light relative to the crystallographic axes [13, 14]. Based on this characteristic polarization-dependent Raman intensity the crystal orientation in some materials has been determined [15, 16]. Lu et al. [17] investigated high temperature electron cyclotron resonance (ECR) PECVD samples with f over 72%. Its application in determining preferred orientation of crystals in complex mixed-phase radio frequency plasma enhanced chemical vapor deposition, rf PECVD nc-Si:H has not been reported to our knowledge. Hence, it is necessary to authenticate this approach in low temperature nc-Si:H films over a wider range of materials in terms of the crystal composition.

In this contribution, we demonstrate the possibility of determining the dominant crystal orientation in nc-Si:H based on the analysis of polarized Raman spectroscopy (PRS) measurements. The intensity of the Raman peaks in the spectrum depends on the lattice vibration, which are in turn dependent on the polarization direction of the incident laser light and on the crystallographic grain orientations. It is this Raman intensity dependence on polarization of the incident laser light that is used to determine preferred orientations in crystals [18, 19]. The polarized Raman spectra of standard test silicon wafers of known orientations are used as references and the spectra of our nc-Si:H films are compared to a profile comprising a superposition of the three profiles obtained from the test reference wafers namely (111), (110) and (100) c-Si wafers. The comparison is based on the fit parameters obtained from a least-square fitting routine developed for the purpose. Results from this approach are compared to results obtained from XRD measurements.

In the first section of this paper, a general introduction is given followed by a theoretical background to Raman measurement and PRS in the second section. In section 3 details of the deposition conditions of the experimental samples are laid out. The procedure followed for the Raman and X-ray diffraction measurements are presented. Section 4 contains a description of the approach followed in order to calibrate and validate our measurement results. Measurements results are presented and discussed in section 5. The fitting procedure adopted is explained with the assumptions on which this is based. The fitting parameters obtained from the nc-Si:H samples are compared with that from standard wafers to give indication of the preferred crystal orientation.

2. Theoretical background to Raman and Polarized Raman measurement

The Raman effect was first discovered by Chandreshra V. Raman in 1928 [20]. Raman spectroscopy is a fundamental method by which the structure and composition of materials are probed. It is based on the fact that light scattered inelastically on interaction with a molecule reveals the characteristic nature of the molecule. For elastically scattered light the incident photons have the same energy (frequency) as the scattered photons and this is the case for most of the scattering processes observed [21]. A small fraction of the scattered photons will have an energy which is different from the energy of the incident photon. This energy change induced by the Raman effect in materials is represented graphically as a function of the intensity of the scattered light in the Raman spectrum. The energy change often referred to as Raman shift is expressed in wave numbers (inverse of wavelength) and relates directly to the vibrational frequency of the material.

In the Raman spectrum, the Raman shift expresses the frequency shift between the incident laser light and the scattered light as [21]:

$$\Delta\nu(cm^{-1}) = \nu_L - \nu_R = \frac{10^7}{\lambda_L(nm)} - \frac{10^7}{\lambda_R(nm)} \quad (1)$$

where ν_R and ν_L represents the absolute wave number of the scattered light and that of the laser respectively. ν_L has a fixed value depending on the laser; ν_L = 19455 cm^{-1} for 514 nm line of Ar green laser and 15798 cm^{-1} for the 633 nm line of a HeNe red laser.

In thin-film silicon research, Raman spectroscopy has been used both for qualitative and quantitative micro-structural analysis. It is one of the easiest methods by which the crystalline mass fraction of amorphous and nanocrystalline materials are determined. Also, qualitatively, it can give an indication of the different phase materials ranging from the amorphous, amorphous-to-nanocrystalline transition and the full crystalline phase materials as shown in figure 1. Typically, nc-Si:H film has a Raman spectrum with a peak at around 520 cm^{-1} as in c-Si depending on its crystalline mass fraction and an asymmetric broadening of its width and a tail towards lower wave numbers.

Polarized Raman spectroscopy (PRS) for investigating crystal orientation is based on the fact that the intensity of the Raman scattered light depends on the polarization of the incident laser light relative to the crystal axes of the material being irradiated [22].

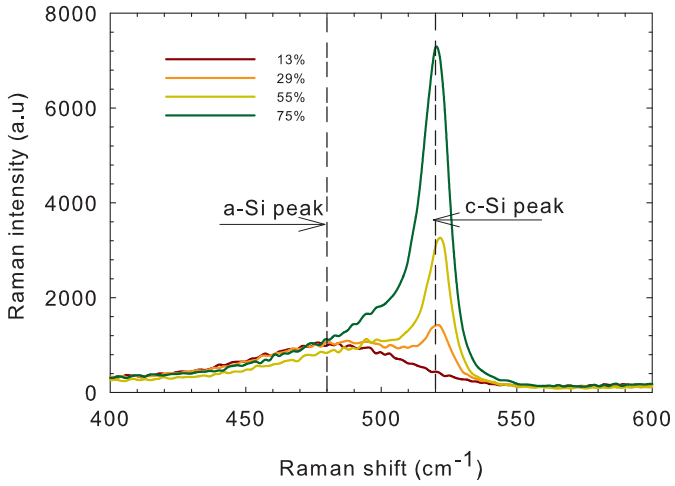

Fig. 1. Raman profile of different phases of thin film silicon-based materials. The peak gets narrower as film crystalline mass fraction increases. Shifting peak position for different f (the legend) implies phase changes. The (TO) mode position in c-Si and a-Si:H are respectively 520 and 480 cm^{-1}.

At fixed sample position the change in the intensity of the scattered light is guided by the symmetry selection rules of the sample and gives information concerning the sample crystal orientation [22-24].

3. Experimental details

The nc-Si:H films used in this experiment were deposited in the rf PECVD set up in the PVMD laboratory, Delft. Intrinsic nanocrystalline silicon layers were deposited on Corning glass (E2000) under varying silane concentration, *Sc* (*Sc* = $SiH_4/(SiH_4+H_2)$), while keeping the deposition pressure and substrate temperature at 9 mbar and 180 ^oC, respectively. The deposition power was also fixed at 542 mW/cm^2. The silane concentration varied between 1.2 to 1.7%. With these deposition conditions we obtained films with *f* in the range 10 to 76%. The crystalline mass fraction was extracted from the Raman spectrum by using a peak-fitting approach to the model of

Smit *et al*. [12]. The thicknesses of the layers were deduced from reflection and transmission measurements by fitting the interference fringes. For all experiments, the thicknesses of the nc-Si:H layers were between 500 and 700 nm. Two crystallized a-Si:H samples deposited by the expanding thermal plasma (ETP) technique were also investigated.

The Raman spectra of the films were measured using a Raman microscope (Renishaw InVia, grating 1800 lines/mm) in a 180^o back scattering geometry with a 25-

mW Ar laser at a wavelength of 514 nm focused on a spot of about 1 μm.

For measurements under different polarization, a change in the polarization of the light is induced by a rotator incorporated in the system and placed in between the laser and spectrometer. The rotation angle was varied in steps of 2^o from 0 to 120^o. Due to a limitation in the turning mechanisms of the rotator, no measurements were recorded beyond 120^o. The incoming light was incident on the sample surface along the *z* axis at 0^o which corresponds to the direction perpendicular to the sample surface.

PRS was first carried out on single crystalline silicon wafers of [111], [110] and [100] orientations in order to establish the dependence of Raman intensities at the 520 cm^{-1} TO peak on rotation angle. We have chosen this phonon band because of its extreme sensitivity to local lattice characteristics [25]. Subsequently, measurements were carried out on all nc-Si:H samples for different polarization angle. For a reference randomly-oriented sample (RD), we measured crystalline silicon powder with particle size below 100 nm. For all PRS profiles, the effect of changing polarization angle on the Raman intensity was corrected.

For purposes of comparison, the preferred crystal orientation of nc-Si:H films was also determined by XRD analysis using an automatic powder diffractometer X'pert Pro with a thin film attachment (parallel beam, asymmetric geometry, fixed incident angle ω, 2θ-scan) and a proportional detector. Copper Kα characteristic radiation (λ = 0.154 nm) was used. The angle of incidence was fixed to 0.5^o and the detector moved with a constant step of 0.05^o from 15 to 65^o on the 2θ scale. The counting time was 20 seconds per step and the irradiated area of the sample was 15×15 mm^2.

4. Raman system calibration and validation test

For each set of PRS measurements, we first carried out a system calibration and validation of the instrument response. The aim is to monitor and possibly correct for any system-induced effects in the measured Raman spectrum. To validate the Raman intensities, we followed the procedure as proposed by McCrery [9]. First we carried out reference measurements on a standard test sample, which in our case is a monocrystalline (110) silicon wafer to check for Raman intensity reproducibility and shift in peak intensity position. These effects can be corrected by an automated system calibration and sometimes with an auto-alignment of the laser. With the angular-dependent polarization measurement, a further calibration and correction was implemented. We checked the effect of the rotation of the rotator on the incident laser intensity by measuring the current generated on a photo-diode for each rotation step [19]. Using the linear dependence of the measured current on laser intensity [25] the Raman spectra were corrected for the laser intensity dependence on rotation angle. We have assumed that this correction takes care of all the rotation-induced effects that may arise from each of the relevant system components [9]. Becker *et al.* [19] have also shown that the grating effect on the Raman scattered light has no influence on the deduced crystal orientation from the Raman measurement. All Raman measurements were carried out at 5% of laser power, which is a pre-determined value at which we observed no laser-induced structural changes in our samples. In order to further validate our method, we checked for the inherent rotational symmetries of the silicon crystals in the different Si wafers. We manually rotated the wafers about the *z*-axis through 360^o and carried out PRS measurements at angular intervals of 90^o until full rotation.

Fig. 2 shows the Raman spectrum of (110) reference wafer used for the calibration of the system. These measurements were taken after carrying out an in-built system check and calibration, which examines the laser alignment and that of all the other components in the path of the laser propagation. We observed that the shift in the crystalline silicon peak position is around 1 cm^{-1},

which is within the acceptable deviation value reported in literature [12, 21]. The linearity of the Raman intensity with the laser power is also established in this figure. Similar result (not shown) is observed for both (111) and (100) silicon wafers except for the differences in the Raman intensity count and associated broadening.

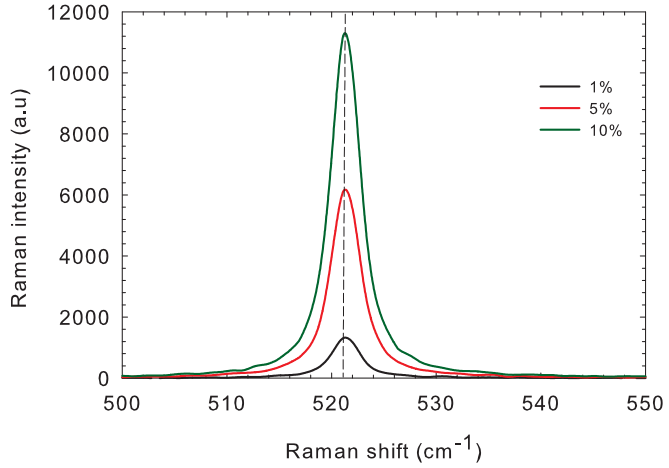

Fig. 2. Raman intensity variation for 1%, 5% and 10% of the full laser intensity carried out on a (110) silicon wafer. The peak position deviates by about 1 cm^{-1} from the 520 cm^{-1} TO peak of crystalline silicon.

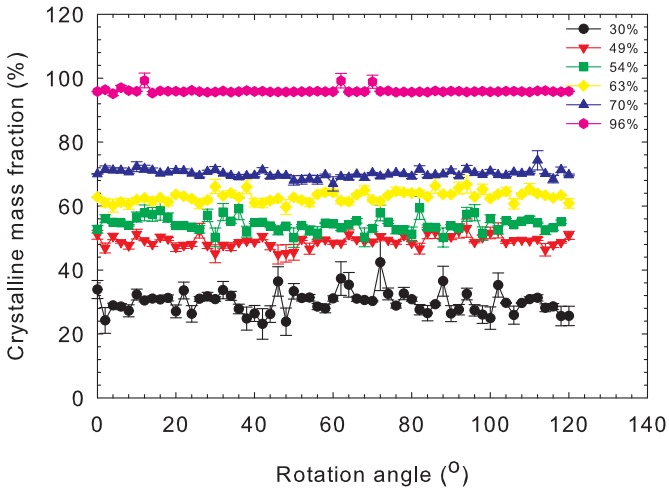

Fig. 3. Crystalline mass fraction, f verses rotation angle for some selected experimental samples. The legend represents the crystalline mass fraction at 0 degree polarization.

To check for the effect of PRS measurement-induced change on the structural property of measured nc-Si:H films, we compared the values of *f* obtained for each rotation angle investigated. A wide range of nc-Si:H samples with crystalline mass fraction ranging from 30 to about 70% were used and the results are presented in figure 3. Here we observe that for all investigated films, *f is* not affected by the PRS measurement as it shows no systematic dependence on the rotation angle. However, the figure also indicates an increasing scattering in the relation between *f* and rotation angle as the material changes from the highly crystalline to the amorphous regime. This can be tied to peak-fitting inaccuracies as the crystalline peak gets smaller with increasing amorphous fraction of the films. Non-dependence of *f* on rotation angle further indicates that there are no measurement-induced structural changes in the materials.

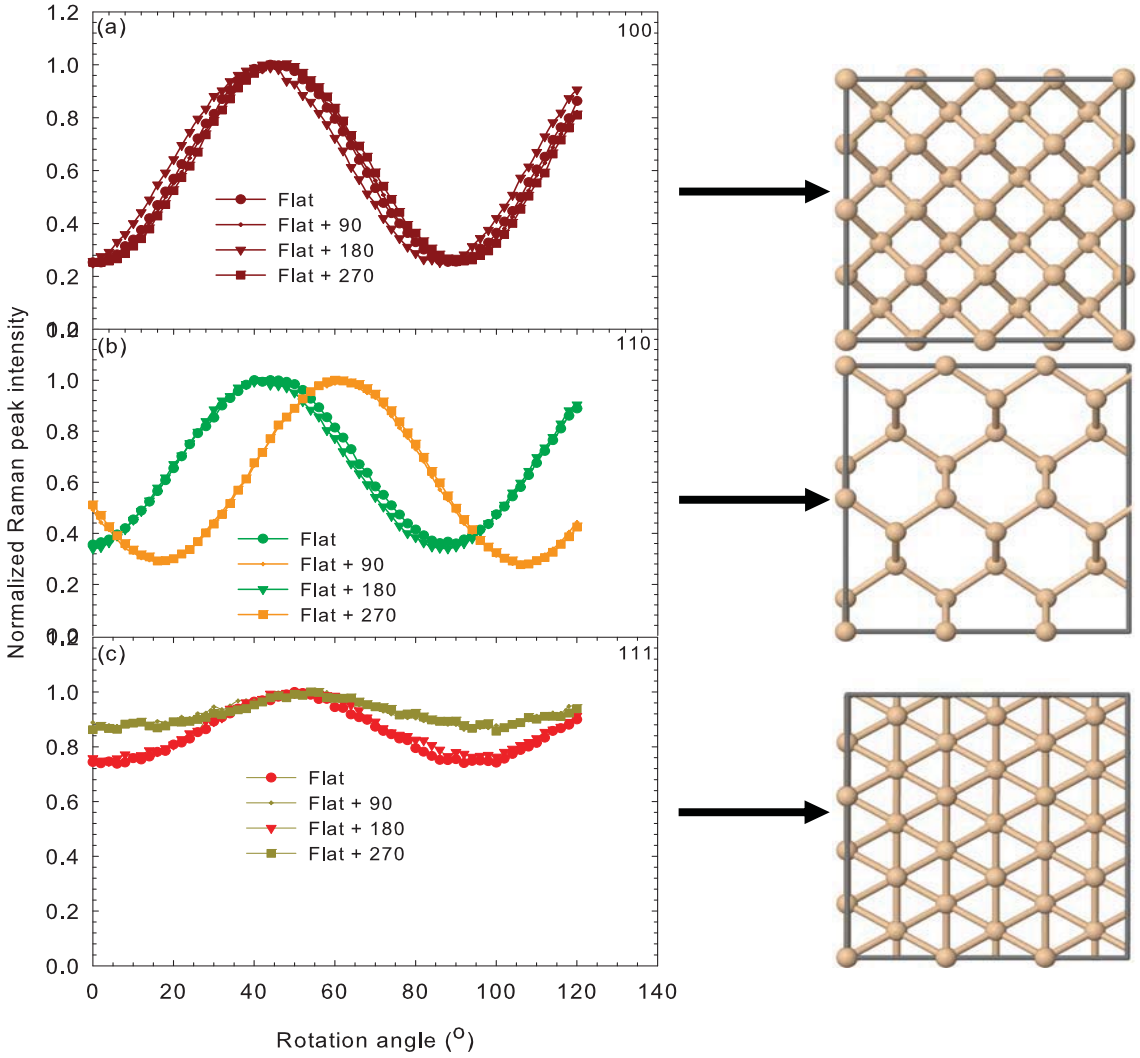

Fig. 4. PRS profile of (a) (100) (b) (110) and (c) (111) c-Si test wafers. Flat as in the legend refers to the primary flat.

Figure 4 shows the PRS profile of the three test wafers taken to test for the rotational symmetry of the wafers. Here we observe that the amplitude of PRS profiles differs for the three different wafers. It decreases as the number of intercepting axes in the test c-Si wafers increases hence (100) profile has the highest amplitude for varying polarization angle and the (111) has the least. We observed that (100) maintains its four-fold symmetry since for the complete wafer rotation the PRS profile remains the same [26]. The peak intensity variation as a function of rotation angle shows a consistent maxima and minima points at around 45° and 90° respectively. The (110) and the (111) show two-fold rotational symmetry for each 180° rotation. The well-known 3-fold rotation symmetry of the (111) wafer [27] can be observed from the similar Raman intensity value at 0 and 120° rotation. While the (110) PRS profile indicates a shift in the maxima and minima points position for each rotation symmetry, the (111) maintains its maxima and minima positions for all rotations with much lower amplitude than both the (100) and the (110). This is a further indication that PRS profiles are unique depending on the crystallographic structure of the irradiated samples.

5. Results and discussion

5.1 Data analysis

In analyzing the PRS measurement data, we use a relatively simple qualitative approach to determine preferred crystal orientation in nc-Si:H films. The analysis of the PRS measurement data involves least square fitting of the measured nc-Si:H profile to a unique profile obtained by superposition of (111), (110) and (100) data profiles obtained from the respective monocrystalline silicon wafers. The following assumptions were made:

1. Thin film nc-Si:H are composed of nano-crystals embedded in the amorphous matrix. The mass fractions of these crystals are expressed as a percentage of the entire material composition.
2. The structural properties of nc-Si:H are derived from the properties of its constituents. Hence we consider nc-Si:H to be a linear system. The constituents include crystal grains of varying orientations, grain boundaries, voids and the amorphous matrix. However, we consider only the crystal orientation, crystalline mass fraction and the amorphous matrix as Raman-active constituents.
3. The mixed-phase nature of nc-Si:H implies that its constituents retain their individual properties, thus they are independent and as such nc-Si:H can be treated as a linear system.
4. The most commonly detected crystal orientations in nc-Si:H are [111], [220] and [311], with the dominant orientation often being [111] or [220]. Based on this and also on the fact that we have reference crystalline silicon wafers only in [111], [110] and [100] orientations, our model is limited to detect only to these dominant orientations. In our approach, we take [110] to be equivalent to [220] except for the differences in their interplanar distances.
5. We assume that there is no contribution of the amorphous fraction to the preferred orientation in nc-Si:H.

If we consider mixed-phase nc-Si:H as a linear system, then we can apply the superposition principle as follows:

$$I_{nc}(\alpha) = a_{111} I_{111}(\alpha) + a_{110} I_{110}(\alpha) + a_{100} I_{100}(\alpha) \tag{2}$$

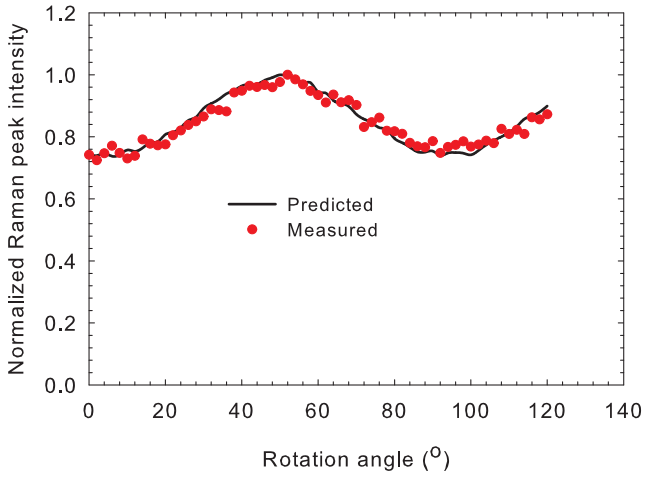

Fig. 5. A comparison between experimental data obtained from the PRS measurement and a predicted data obtained from equation (1). The profile is that of a nc-Si:H sample with f ~ 63%.

where I_{nc}, I_{111}, I_{110}, I_{100} are the normalized Raman intensity at 520 cm^{-1} TO peak as a function of rotation angle α, for the experimental nc-Si:H films and the (111), (110) and (100) test wafers

respectively. a_{111}, a_{110} and a_{100} are best-fit parameters which are obtained on fitting I_{nc} to equation (2) by least square fitting algorithm. The best-fit parameters are obtained as unique parameters on a boundary condition that their summation equals one and the least possible residual deviation from the experimental values is obtained. A very good agreement between the measured and the fitted profiles is obtained for most of the films. An example is presented in figure 5.

In order to further verify our model, several *goodness-of-fit* tests are carried out. These are standard statistical model validity tests [28, 29] based on the residual, R, which is the difference between the observed and predicted value estimated from the regression equation. The least squares method chooses the parameter estimates such that the sum of the squared residuals is minimized. *Goodness-of-fit* tests employed in this work include the sum of squares of the residual R^2, correlation coefficient *CC*, root mean square error *RMSE*, and the mean bias error, *MBE*. The detailed formulae of these tests as applied here are described in detail elsewhere [28]. For a good fit, R^2 and the error values of *RMSE* and *MBE* approach zero. *CC* has values between 0 and 1 and gives indications of linearity of relationship between the dependent and the independent variables. A value of 1 implies a perfect fit and a strong relationship, while 0 means a bad fit and absence of any relation. Table 1 shows a summary of the test of validity indices and the fit parameters. This will be discussed in section 5.3.

Table 1. Details of the fit parameters obtained from the model of equation (1) and the goodness-of-fit test results for all the test samples. E1 and E2 are thin film silicon samples deposited by expanding thermal plasma (ETP) and R1 to R8 are nanocrystalline silicon samples deposited using rf PECVD.

Sample ID	f	Fit parameters			Test of validity indices			
	(%)	a_{111}	a_{110}	a_{100}	R^2	*RMSE*	*CC*	*MBE*
[111]	-	1.0000	0.0000	0.0000	0.0000	0.0000	1.0000	0.0000
[110]	-	0.0000	1.0000	0.0000	0.0000	0.0000	1.0000	0.0000
[100]	-	0.0000	0.0000	1.0000	0.0000	0.0000	1.0000	0.0000
RD	96	1.0000	0.0000	0.0000	0.9062	0.1219	0.7318	-0.1014
R1	30	0.6765	0.0000	0.3235	0.3716	0.0781	0.8741	0.0361
R2	49	0.9664	0.0000	0.0336	0.0512	0.0290	0.9570	0.0105
R3	54	0.9865	0.0135	0.0000	0.0268	0.0210	0.9719	0.0016
R4	60	0.8619	0.0000	0.1381	0.1858	0.0552	0.8877	0.0240
R5	63	1.0000	0.0000	0.0000	0.0594	0.0312	0.9748	-0.0238
R6	67	0.8766	0.1234	0.0000	0.0557	0.0302	0.9544	0.0022
R7	70	0.9645	0.0000	0.0355	0.0202	0.0182	0.9805	0.0028
R8	73	1.0000	0.0000	0.0000	0.0448	0.0271	0.9755	-0.0193
E1	92	0.8809	0.0993	0.0198	0.1657	0.0521	0.8691	0.0147
E2	95	0.9074	0.0926	0.0000	0.0722	0.0344	0.9374	0.0039

5.2 PRS spectra for (111), (110) and (100) reference silicon wafers.

The Raman intensity at 520 cm^{-1} as a function of rotation angle normalized to the maximum intensity is presented in figure 6 for the three silicon wafers and silicon powder (RD). Because our interest is in relating the Raman profile of the silicon wafers of known crystal orientation to the profile obtained in nc-Si:H films we limited our comparison to measurements taken along the *z*-axis perpendicular to the primary flat because the primary flat has specific orientation relative to the wafer surface [30] and is present in all the test wafers. The variation in rotation angle results in a change in the polarization plane of incident light and hence affects the Raman scattering intensity [31]. We attribute this to the different degrees of scattering and energy distribution within the crystal lattice of the silicon wafers depending on the crystal plane. The <111> plane has the largest number of silicon atoms per cm^2 (atomic lattice packing density)

whereas <100> has the least number of atoms per cm^2 [32, 33]. If the bond density in the intercepting plane is high, this will result in a more even distribution of the Raman intensity with rotation angle, as more interactions between the plane and incident laser light are more likely. The least dependence of Raman intensity on rotation angle observed for the (111) wafer implies a more even distribution of the scattered light since it also has more bonds within the lattice than the (110) and the (100) lattices. Similarly, the (100) lattice has the least atomic bonds in its crystallographic structure and thus scatters the least of the incident light. RD shows no clear dependence on the laser polarization, which actually is due to its random structure as has also been earlier observed [17].

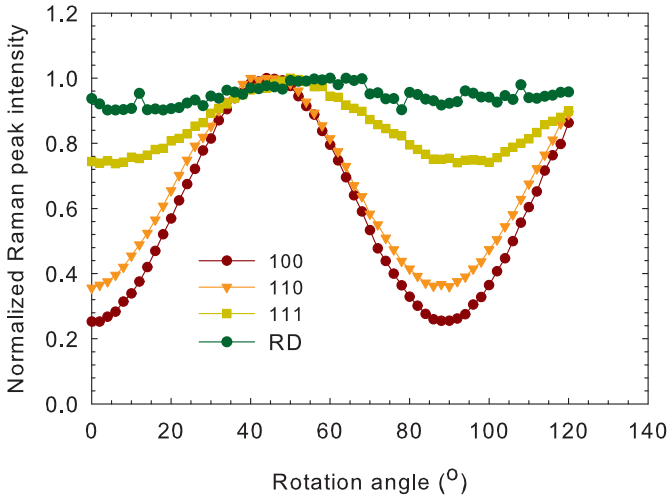

Fig. 6. PRS profile of (111), (110) and (100) test monocrystalline silicon wafers and silicon powder (RD).

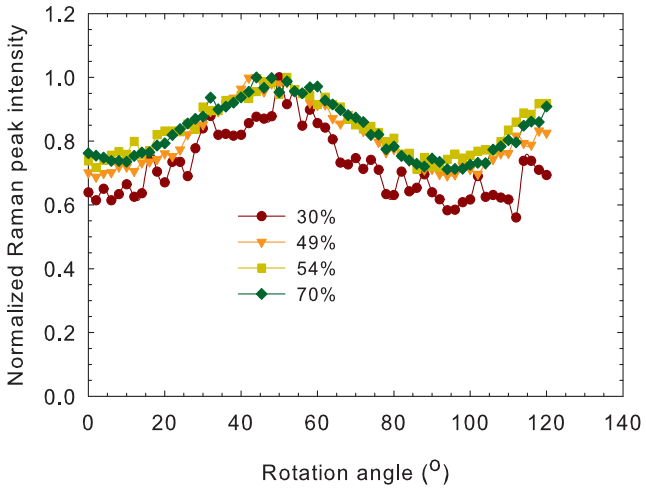

Fig. 7. The PSR profile of selected nc-Si:H samples. The samples' crystalline mass fractions taken at 0 degree rotation are indicated in the legend.

5.3 Predicting dominant crystal orientation in thin film nc-Si:H from Raman polarization spectra of reference test wafers

In Fig. 7 the PRS results of some of the experimental nc-Si:H films of different *f* are presented. A visual comparison of the plots of figure 7 shows that most of the nc-Si:H films have a profile similar to that of (111) Si wafer, which indicates that the films have mainly preferential

[111] orientation. The fit parameters obtained for all the samples are shown in table 1 and are compared to the fit parameters of the test silicon powder, which we consider to have randomly-oriented crystals. Quantitatively, the orientation with the highest value of the fit parameter implies that such orientation is dominant in the film. From table 1 we observe that most of the test samples indicate the dominance of a [111] orientation with a_{111} values of about 90% or higher. For the film with f = 30% as in R1, a_{111} is still the highest fit parameter but drops to 0.677. These fit parameters are adjudged as correct by considering the test of validity indices. The near-zero values of R^2, RMSE and MBE indicate that the fitting error is minimal and high *CC* implies a strong correlation between the predicted and the experimental data. The fit parameters for RD suggest it has a dominance of [111] orientation. However, the *goodness-of-fit* test indicates that the fitting here falls below accepted values for a good fit. This is corroborated by the over 90% value of R^2 and the lower *CC* value.

5.4 XRD analyses of test nc-Si:H films and comparison of results with Raman results

In Fig. 8, the result of the semi-quantitative XRD phase analysis carried out on all significant diffraction lines in 2ϑ-interval of 15-65 degrees of the test samples are presented. The figure 8(a) indicates that all films have a strong [111] orientation finger prints as the strongest peak and is observed at 2ϑ ~ 28°. The I(220)/I(111) intensity ratio is in the range: 0.53 - 0.81. This indicates that the nano-crystals have preferential orientation in the [111] direction; a feature in line with nc-Si:H deposited at the conditions described in section 3 [2]. The (111) intensity increases as f also increases in the films.

Table 2. Comparison between the crystalline mass fraction obtained from Raman and that obtained from XRD.

f (%)		Crystal size (nm)
Raman	XRD	XRD
30	24	4.3
49	62	8.0
54	47	9.7
63	47	13.5
70	74	16.3
73	75	11.4

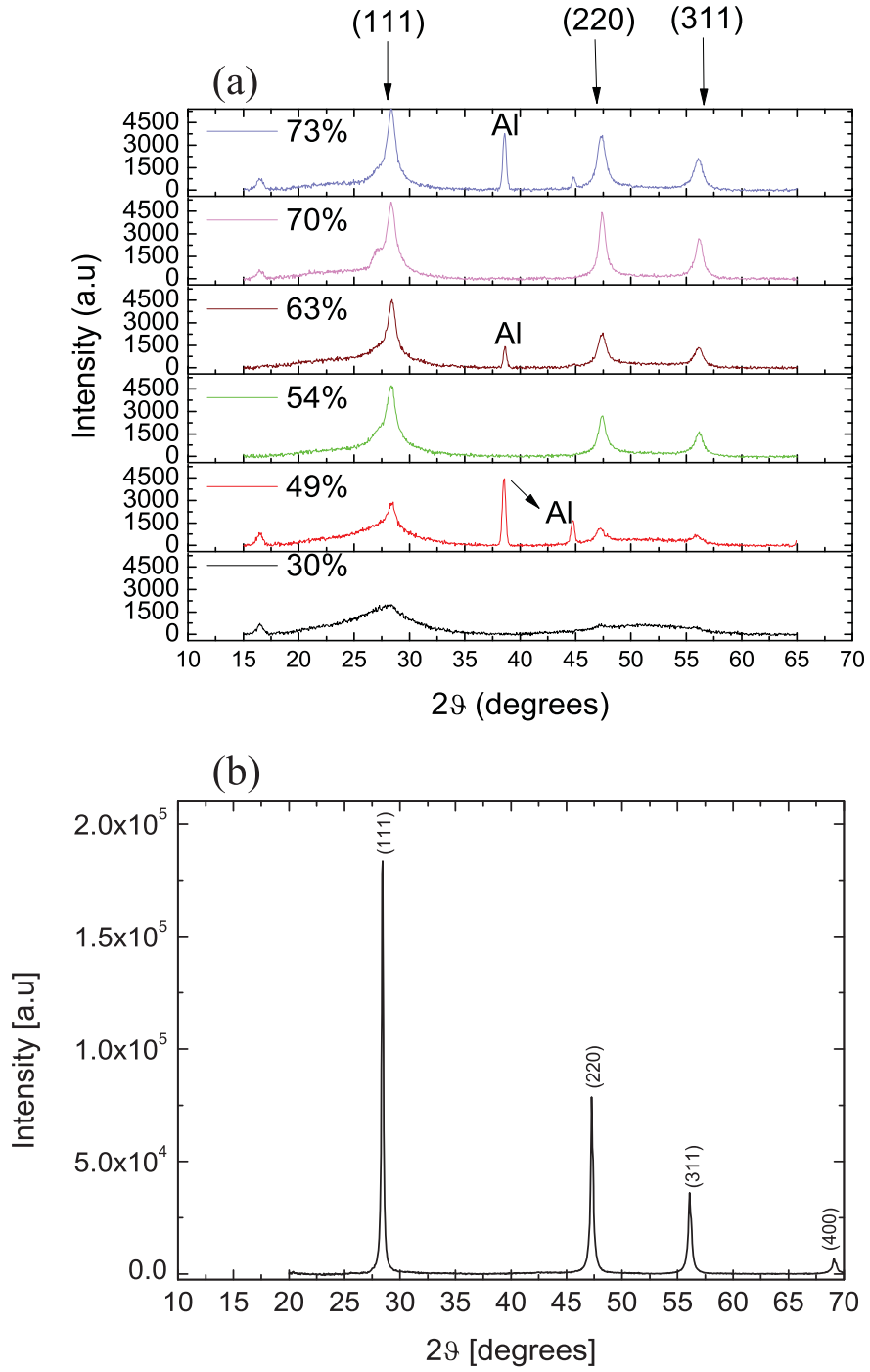

Fig. 8. X-ray diffraction patterns of (a) nc-Si:H samples of different crystalline mass fraction, f (b) nanocrystalline silicon powder (RD). The legend in figure 8(a) represent the f value of each nc-Si:H sample.

The broadening of the (111) peak and its lower intensity for the material with $f = 30\%$ for instance is indicative of the amorphous fraction. Figure 8(b) shows the XRD pattern of the test random sample (silicon powder). In figure 8(b) we observe that the I(220)/I(111)) intensity ratio has a value of about 0.4 which indicates a much higher (111) intensities in the test random sample than in the nc-Si;H samples in figure 8(a). This suggests that the [111] oriented crystals mainly dominates the powder.

A comparison between *f* values obtained from Raman and that from XRD is presented in table 2. The *f* values from XRD were estimated by comparing integrated intensities of amorphous

and crystalline components of the XRD patterns after separating the overlapped diffraction lines by curve fitting. Good agreement is observed for some samples, especially for the highly crystalline samples. The difference between *f* obtained from Raman and from XRD has also been earlier reported [34] and has been ascribed to the difference in the depth probed and in the sensitivity of the techniques. From the XRD results crystallite size (see table 2) was evaluated using (001) silicon hydride line and (111) silicon line. Crystal sizes in the range 4-17 nm were obtained and they seem to become larger as *f* increases.

6. Conclusion

The use of Polarized Raman Spectroscopy for the investigation of preferred orientation of crystals in nc-Si:H has been demonstrated. This principle is based on the fact that polarized laser light on interaction with crystalline material of a given crystallographic structure generates a unique scattering profile which can give insight into the orientation of the irradiated crystals. Based on this we have investigated a wide range of nc-Si:H samples. These samples had crystalline mass fractions ranging from the 30 to over 70% and were mainly deposited using rf PECVD. For this work we have used the (111), (110) and (100) monocrystalline silicon wafers as reference orientations and obtained distinct PRS profiles for each wafer. We have applied the superposition principle by fitting the PRS profiles of our nc-Si:H samples to a linear combination of (111), (110) and (100) profiles. Using a least-squares fitting algorithm we inferred the preferred orientation of our nc-Si:H samples by comparing the fit parameters. Our results show that most of the samples have mainly a [111] preferred orientation and this is well corroborated by XRD measurements. This approach is simple and faster than other techniques used for inferring the orientation of crystals in nc-Si:H.

Acknowledgements

The authors are grateful to the Netherlands Fellowship Programme for supporting the research of Solomon Agbo. This work was also supported within the CENTEM project, reg. no. CZ.1.05/2.1.00/03.0088 that is cofunded from the ERDF within the OP RDI programme of the Ministry of Education, Sports and Youth of the Czech Republic and by the project No. 1M06031.

References

[1] T. Kaneko, M. Wakagi, K. Onisawa, T. Minemura, Appl. Phys. Lett. **64**, 1865 (1994).
[2] H. Kakinuma, J. Vac. Sci. Technol. A **13**, 2310 (1995).
[3] J. Müllerovà, S. Jurečka, P. Šutta, Optical Sol. Energy **80**, 667 (2006).
[4] L. Houben, M. Luysberg, P. Hapke, O. Vetterl, F. Finger, R. Carius, H. Wagner, J. Non-Cryst. Solids **227-230**, 896 (1998).
[5] J. Bailat, E. Vallat-Sauvain, L. Feitknecht, C. Droz, A. Shah, J. Non-Cryst. Solids **299-302** 1219 (2002).
[6] Y. Sobajima, S. Nakano, M. Nishino, Y. Tanaka, T. Toyama, H. Okamoto, J. Non-Cryst. Solid **354**, 2407 (2008).
[7] N. Takesue, H. Chen, J. Appl. Phys. **76**, 5856 (1994).
[8] H. S. Fong, J. Material Sci. **22,** 2363 (1987).
[9] R. L. McCreery, Raman spectroscopy for chemical analysis, John Wiley and Sons, Inc., Canada, 2000.
[10] N. Hayazawa, M. Motohashi, Y. Saito, H. Ishitobi, A. Ono, T. Ichimura, P. Verma, S. Kawata, J. Raman Spectrosc. **38**, 684 (2007).
[11] I. De Wolf, Semicond. Sci. Technol. **11**, 139 (1996).
[12] C. Smit, R. A. C. M. M. van Swaaij, H. Donker, A. M. H. N. Petit, W. M. M. Kessels M. C. M. van de Sanden, J. Appl. Phys. **94**, 3582 (2003).
[13] K. Mizoguchi, S. Nakashima, J. Appl. Phys. **65**, 2583 (1989).
[14] T. V. Basova and B. A. Kolesov, Thin Solid Films **325**, 140 (1998).

[15] J. Dowdy, J. J. Hoagland, K. W. Hipps, J. Phys. Chem. **95**, 3751 (1991).
[16] N. E. Schlotter, J. F. Rabolt, J. Phys. Chem. **88**, 2062 (1984).
[17] Z. Q. Lu, T. Quinn, H. S. Reehal, J. Appl. Phys. **97**, 033512 (2005).
[18] W. Salcedo, F. Fernandez, J. Rubim, J. Raman Spectrosc. **30**, 29 (1999).
[19] M. Becker, H. Scheel, S. Christiansen, H. P. Strunk, J. Appl. Phys **101**, 063531 (2007).
[20] C. V. Raman, K. S. Krishnan, A new type of secondary radiation, Nature **121**(3048), 501 (1928).
[21] C. Droz, Thin film microcrystalline silicon layers and solar cells: microstructure and electrical performances, PhD thesis, University of Neuchatel, 2003.
[22] W. Hayes, R. Loudon , Scattering of light by crystals. Wiley, New York, 1978.
[23] J. B. Hopkins, L. A. Farrow, and G. J. Fisanick, Appl. Phys. Lett. **44**, 535 (1984).
[24] G. Kolb, T. Salbert, and G. Abstreiter**,** Fresnel J. Anal Chem. **341**, 166 (1991).
[25] J. B. Hopkins, L. A. Farrow, J. Appl. Phys. **59**, 1103 (1986).
[26] http://en.wikipedia.org/wiki/Crystal_structure. (Accessed: 10 November, 2012).
[27] A. Dadgar, F. Schulze, M. Wienecke, A. Gadanez, J. Blasing, P. Veit, T. Hempel, A. Diez, J. Christen, A. Krost, New J. Phys. **9**, 389 (2007).
[28] M. Iqbal, An Introduction to Solar Radiation. Academic Press: Toronto, Canada, 1983.
[29] C. Huang, Regression and correlation based on the method of least percentage squares, J. Atmospheric and terrestrial physics 26 (1964) 959.
[30] http://www.phy.duke.edu/~hx3/physics/silicon/silicon.htm (Accessed: 11 September, 2012).
[31] G. Irmer, J. Appl. Phys. **76**, 7768 (1994).
[32] B. Sharma, Crystal growth-bulk and epitaxial film-part 3, http://cnx.org/content/m34202/1.2 (Accessed: 23 November, 2012).
[33] A. E. Franke, Fabrication of extremely smooth nanostructures using anisotropic etching, M. Sc Thesis, Massachusetts Institute of Technology, 1997.
[34] A. M. Funde, N. Ali Bakr, D. K. Kamble, R. R. Hawaldar, D. P. Amalnerkar, S. R. Jadkar, Sol. Energy Mater. Sol. Cells **92**, 1217 (2008).